

# Spatially Resolved Low Frequency VLA observations of the Supernova Remnant 3C 391

C. L. Brogan<sup>1,2</sup>, T. J. Lazio<sup>3</sup>, N. E. Kassim<sup>3</sup>, and K. K. Dyer<sup>3,4</sup>

## ABSTRACT

We present VLA images of the supernova remnant (SNR) 3C 391 at 74, 330, and 1465 MHz. This remnant has been known for some time to exhibit a turnover in its integrated radio continuum spectrum at frequencies  $< 100$  MHz, indicative of free-free absorption from thermal ionized gas along the line of sight. For the first time, our data reveal the spatially resolved morphology of the low frequency free-free absorption with a resolution of  $\sim 70''$ . Contrary to the expectation that such absorption arises from unrelated low density H II regions (or their envelopes) along the line of sight, these data suggest that in this case the absorbing medium is directly linked to the SNR itself. 3C 391 has been shown in a number of recent papers to be interacting with a molecular cloud. Indeed, it exhibits a number of signposts of SNR/molecular cloud shocks including OH (1720 MHz) masers and broad molecular emission lines. Comparison of the regions of strongest 74 MHz absorption with existing X-ray, IR, and molecular data suggests that the free-free absorption originates from the SNR/molecular cloud shock boundaries due to ionized gas created from the passage of a J-type shock with a speed of  $\sim 100$  km s<sup>-1</sup>. This makes only the second SNR for which such (extrinsic) spatially resolved absorption has been measured, and the only one for which the absorption is thought to arise from a SNR/molecular cloud interface region.

*Subject headings:* supernova remnants — ISM: molecules — ISM: individual (3C 391)

---

<sup>1</sup>University of Hawaii, Institute for Astronomy, 640 North A'ohoku Place, Hilo, HI 96720; cbrogan@ifa.hawaii.edu

<sup>2</sup>James Clerk Maxwell Telescope Postdoctoral Fellow

<sup>3</sup>Naval Research Laboratory, Remote Sensing Division, Code 7213, 4555 Overlook Avenue SW, Washington, DC 20375-5351; joseph.lazio@nrl.navy.mil; namir.kassim@nrl.navy.mil; kdyer@nrao.edu

<sup>4</sup>NRC Postdoctoral Fellow

## 1. INTRODUCTION

Supernovae have a profound effect on the morphology, kinematics, and ionization balance of galaxies. The impact of supernova shocks on surrounding molecular clouds may also trigger new generations of star formation. The idea that cosmic-rays (up to  $\sim 10^{14}$  eV) are produced by shock acceleration in supernova remnants (SNRs) has recently gained wide acceptance (e.g. Jones *et al.* 1998). Although the details of the SNR cosmic-ray acceleration process remain uncertain, many of the current models predict spatial variations in the spectral indices of SNRs at the sites of cosmic-ray acceleration (c.f. Reynolds & Ellison 1992). The spectral index variations predicted by many of these models are most easily discerned at low radio frequencies. There is also evidence that some of the low latitude unidentified EGRET  $\gamma$ -ray sources may be associated with sites of SNR/molecular cloud interactions, implying that these sources are particularly efficient at producing high energy cosmic-rays (see for example Torres *et al.* 2003). Thus, sites of SNR/molecular cloud interaction represent a promising place to look for signatures of shock acceleration. However, unambiguous evidence for SNR/molecular cloud interactions is difficult to find due to Galactic velocity confusion in the low- $J$  molecular lines generally used for such searches, so that only a handful of such sources are currently known (c.f. Reach *et al.* 2002).

A further complication is the determination of whether observed spectral index variations are intrinsic to the synchrotron emission, or are affected by other processes. Using integrated flux measurements, Kassim (1989b) found that  $\sim 2/3$  of Galactic SNRs undergo a spectral turnover for frequencies  $\lesssim 100$  MHz. These low frequency turnovers have been attributed to free-free absorption in low density  $n_e \sim 1 - 10 \text{ cm}^{-3}$  intermediate temperature ( $T \sim 5000$  K) ionized thermal gas along the line of sight to the SNR. The ubiquitous detection of low frequency radio recombination lines (RRLs) amplified by stimulated emission, towards almost every direction in the inner Galaxy (e.g. Roshi & Anantharamaiah 2001; Anantharamaiah 1986, 1985) provides further evidence for ionized gas with the requisite densities and temperatures. The nature of the ionized gas remains unclear, with the extended envelopes of normal H II regions being one candidate (also see §4.3, Brogan *et al.* 2004, and references therein). Spatially resolved low frequency observations of SNRs with absorption will be crucial for understanding the origin of the absorbing medium. Also, while such absorption is interesting in its own right for understanding the composition of the ISM, it hinders efforts to look for unambiguous spectral index variations predicted by cosmic-ray acceleration models. Therefore, quantifying the level and origin of free-free absorption toward SNRs is also critical to studies of the cosmic-ray shock acceleration process.

The first spatially resolved observations of extrinsic low frequency absorption toward an SNR were made by Lacey *et al.* (2001) toward W49B using the then recently completed

74 MHz system at the Very Large Array (VLA). These authors found that most of the low frequency absorption implied by previous low resolution integrated flux measurements is confined to the western half of the remnant, and is spatially coincident with a neutral H I column density peak at a kinematic distance well in front of the SNR. Evidence for the requisite ionized gas comes from radio recombination line (RRL) detections at the same velocity as the neutral H I gas. Thus, the synchrotron emission from W49B is absorbed by an unrelated partially ionized cloud along the line of sight.

Based on the interesting W49B result, and recent improvements in low frequency wide-field imaging techniques we have begun a low frequency survey of the inner Galactic plane with the VLA<sup>1</sup> at 74 and 330 MHz. With this study we hope to spatially resolve and characterize the low frequency absorption toward a large sample of SNRs from  $\ell = -10^\circ$  to  $50^\circ$  (see Brogan *et al.* 2004, and Brogan *et al.* 2004, in prep). This paper presents results from this survey at 74 MHz as well as archival VLA data at 330 and 1465 MHz for the SNR 3C 391 (G31.9+0.0). The organization of the paper is as follows: §1.2 describes previous observations of 3C 391, §2 briefly describes the data reduction, §3 describes our results, §4 presents comparisons of our data with previous observations toward 3C 391 and discusses the implications, and our findings are summarized in §5.

### 1.1. Previous observations of 3C 391

From integrated radio flux measurements, 3C 391 has been known from the 1970s to suffer from low frequency absorption (see for example Dulk & Slee 1975). In addition, RRLs (which cannot originate from the synchrotron emission of the SNR) have been detected toward 3C 391 at velocities of  $\sim 100 \text{ km s}^{-1}$  (Pankonin & Downes 1976; Cesarsky & Cesarsky 1973). Reynolds & Moffett (1993) and Moffett & Reynolds (1994) report the results of the first high resolution radio continuum observations toward 3C 391 at 330, 1468, and 4848 MHz (earlier, lower resolution radio frequency studies are also reviewed in these references). At high resolution, 3C 391 displays a rim brightened morphology to the NW with the synchrotron emission gradually fading to the SE, indicative of a “breakout” into lower density gas in this region. Moffett & Reynolds (1994) hoped to find spectral signatures of shock acceleration in the resulting high resolution spectral index maps of 3C 391, but could find no convincing evidence for such variations above their detection limit of  $\Delta\alpha = 0.1$  ( $S \propto \nu^\alpha$ ).

It has recently been discovered that 3C 391 is interacting with a nearby molecular cloud

---

<sup>1</sup>The National Radio Astronomy Observatory is a facility of the National Science Foundation operated under cooperative agreement by Associated Universities Inc.

which also has a velocity of  $\sim 100 \text{ km s}^{-1}$  (Wilner, Reynolds, & Moffett 1998). Further proof of an interaction comes from the presence of OH (1720 MHz) masers which trace SNR/molecular cloud shocks (when the mainline masers are absent; Frail *et al.* 1996). More detailed observations of the associated molecular gas have been carried out by Reach & Rho (1999). These authors find evidence for broad CO linewidths indicative of a shock at the location of one of the OH masers. The distance to the SNR constrained by the velocity of maximum HI absorption (which is equal to that of the tangent point), CO emission line velocities, and the velocities of the OH masers ( $\sim 105 \text{ km s}^{-1}$ ) is  $\sim 7.5 \text{ kpc}$  (Radhakrishnan *et al.* 1972; Wilner, Reynolds, & Moffett 1998; Frail *et al.* 1996). At a distance of 7.5 kpc,  $1'$  is equivalent to 2.2 pc. Extensive near and mid infrared observations of 3C 391 have been carried out by Reach *et al.* (2002) and Reach & Rho (2000) which have yielded further detailed information on the nature of the shock interaction. The results of these studies are discussed further in §4.2.

The X-ray properties of 3C 391 have been studied by Chen *et al.* (2004), Chen & Slane (2001), Rho & Petre (1996), and Wang & Seward (1984) using *Chandra*, ASCA, ROSAT, and *Einstein* respectively. Overall, the X-ray morphology of 3C 391 places it in the “mixed morphology” or “thermal composite” class (Rho & Petre 1998). That is, the X-ray emission is brightest interior to the radio synchrotron shell, with weak or no emission coincident with the radio shell. In all of the X-ray studies described above, the centroid of soft X-ray emission is offset to the SE of the harder X-ray emission. This has been interpreted as an absorption effect due to the extra column density provided by the molecular cloud to the NW (Chen *et al.* 2004; Chen & Slane 2001). Chen *et al.* (2004) find that the column density difference implied by the soft x-ray absorption is  $\sim 6 \times 10^{21} \text{ cm}^{-2}$ . These authors also suggest that if the column density difference is due to the interacting molecular cloud, the implied *average* molecular cloud density is  $\sim 20 \text{ cm}^{-3}$  where they have assumed a cloud depth of  $\sim 12 \text{ pc}$  ( $5'$  at a distance of 8 kpc, comparable to the angular extent of 3C 391). Alternative estimates for the cloud density are presented in §4.3.

## 2. OBSERVATIONS

We observed the supernova remnant 3C 391 using the Very Large Array (VLA) at 74 MHz using the A, B, & C configurations. In addition, we obtained 330 MHz C configuration and 1465 MHz D configuration data from the VLA archive. This combination of configurations provides comparable  $u - v$  coverage at all three frequencies – a prerequisite for believable spectral index calculations. The observing parameters for each frequency are presented in Table 1. The 74 and 330 MHz data were reduced using the wide-field imaging and calibration

techniques described in Brogan *et al.* (2004, , and references therein). The 1465 MHz data were reduced in the usual manner. All data reduction utilized the AIPS software package.

The final resolution of the 74 MHz image after combining the four datasets described in Table 1 is  $70''$ . This resolution is about 2.8 times larger than what is technically feasible from the longest A configuration baseline (30 km). This is due in part to the fact that the A-configuration 74 MHz data were taken under poor ionospheric conditions which caused the longest baselines to have incoherent phases. To mitigate this effect the 74 MHz data were imaged with a  $u-v$  taper of  $5.5\text{ k}\lambda$  (this corresponds to a baseline length of 22 km). In addition, the combination of A+B+C configuration data pushes the final resolution to one that is intermediate (B) between the configuration extremes (A and C). The 330 and 1465 MHz images were convolved to match the  $70''$  of the 74 MHz images. This convolution was minimal for both the C configuration 330 MHz and D configuration 1465 MHz data (each with an unconvolved resolution of  $\sim 60''$  resolution).

Since 3C 391 is located  $2.2^\circ$  from the phase center of the 74 MHz data, primary beam correction was applied to this image (the radius of the FWHM primary beam of the VLA at 74 MHz is  $\sim 5.8^\circ$ ). No primary beam correction was necessary at 330 and 1465 MHz since 3C 391 subtends a small fraction of the primary beam at these frequencies and 3C 391 was located at the phase center of these observations. The rms noise levels achieved in each image are: 75, 15, and 3 mJy beam $^{-1}$  at 74, 330, and 1465 MHz, respectively. Note that these rms noise levels are significantly higher than theoretical, due to imperfect  $u-v$  coverage (especially for the archival data) and Galactic confusion.

### 3. RESULTS

Figure 1a shows our 330 MHz  $70''$  resolution continuum image of 3C 391, while Figure 1b shows a 330/1465 MHz spectral index map of 3C 391. Even at this fairly coarse resolution it is apparent that 3C 391 has a rim-brightened morphology on its western side and has a breakout morphology to the SE indicating that the remnant is unbounded in this region (see Moffett & Reynolds 1994, for higher resolution images). Figure 1c shows the notably different morphology of the 74 MHz emission, while Figure 1d shows the 74/330 MHz spectral index. For both spectral index maps, the images were masked at the  $4\sigma$  level before the spectral index was calculated (we use the definition  $S \propto \nu^\alpha$ ). Neglecting edge effects (the spectral index maps become more uncertain with decreasing continuum brightness), the 330/1465 MHz spectral index map is quite uniform with an average spectral index of  $-0.45$ . The 74/330 MHz spectral index map is dramatically different from the 330/1465 MHz map. Indeed the 74/330 MHz spectral indices are inverted to positive values in a ring

like morphology around the SNR. Such spectral behavior is contrary to that expected of nonthermal emission and is indicative of free-free absorption at 74 MHz, the morphology of which is revealed here for the first time.

Integrated flux density measurements were made for the three frequencies in our study for 3C 391. Since the images have different noise levels, and 3C 391 has a “breakout” morphology to the SE that gradually fades into the noise it was difficult to determine where the boundary of the SNR should be drawn. Therefore, in order to get comparable flux density estimates, the  $4\sigma$  ( $60 \text{ mJy beam}^{-1}$ ) contour of the 330 MHz image (see Figure 1a) was used to define the boundary for all of the integrated flux measurements. The integrated flux densities are  $20.2 \pm 0.1$ ,  $38.9 \pm 0.3$ , and  $28.1 \pm 1.8 \text{ Jy}$  at 1465, 330, and 74 MHz, respectively. The errors on these flux density measurements were estimated by  $(\# \text{ independent beams})^{1/2} \times 3\sigma$  at each frequency.

A plot of the integrated continuum spectrum of 3C 391 is shown in Figure 2 including data from the current work and integrated flux densities from the literature for cases in which an error estimate is available and the error is less than 20%. As described in §1, it has been known for some time that 3C 391 has a low radio frequency turnover, and this effect is quite apparent in Figure 2 for  $\nu < 100 \text{ MHz}$ . In order to determine the properties of the turnover, we have made a weighted least squares fit of the integrated flux densities shown in Fig. 2 to the equation

$$S_\nu = S_{330} \left( \frac{\nu}{330 \text{ MHz}} \right)^\alpha \exp \left[ -\tau_{330} \left( \frac{\nu}{330 \text{ MHz}} \right)^{-2.1} \right], \quad (1)$$

where  $S_{330}$  and  $\tau_{330}$  are the flux density and optical depth at a fiducial frequency of 330 MHz, respectively, and  $\alpha$  is the integrated spectral index (Dulk & Slee 1975; Kassim 1989a). This equation assumes a standard nonthermal constant power law spectrum and allows for a thermal absorption turnover at lower frequencies (see e.g. Dulk & Slee 1975; Kassim 1989a). The free-free continuum optical depth at other frequencies can be estimated from  $\tau_\nu = \tau_{330} \left( \frac{\nu}{330 \text{ MHz}} \right)^{-2.1}$ . The best fit parameters using the data shown in Figure 2 are  $S_{330} = 41.0 \text{ Jy}$ ,  $\alpha = -0.49 \pm 0.1$  and an average optical depth at 74 MHz of  $\tau_{74} = 1.1$ . The average optical depth at 330 MHz is 0.08, indicating that the emission at this frequency is little affected by free-free absorption, although the average 330/1465 MHz spectral index ( $-0.45$ ) is slightly shallower than that calculated from the full spectrum ( $-0.49$ ) due to this effect.

The derived value of the integrated  $\tau_{74} = 1.1$  is about a factor of two larger than that predicted by Kassim (1989b). This discrepancy is due in large part to the fact that the Kassim (1989b) fit includes a  $3\sigma$  30.9 MHz *non-detection* upper limit, whereas we have not included this data point in our fit (although this upper limit does appear on Fig. 2 for

reference). In addition, we also use a weighted least squares fit which places greater emphasis on the more precise flux measurements, including the three new flux measurements from this study. From Figure 2 it is clear that the flux density of 3C 391 at 30.9 MHz is likely to be significantly lower than the  $3\sigma$  30.9 MHz detection limit of the Kassim (1989b) data. Thus, we are confident that this increase in the  $\tau_{74}$  estimate is real, but an even lower frequency *detection* (i.e.  $< 74$  MHz) would better constrain the fit.

## 4. DISCUSSION

### 4.1. Comparison to X-ray morphology

Figure 3a shows hard X-ray emission contours integrated from 2.6 - 10 keV from ASCA (Chen & Slane 2001) superposed on the 74/330 MHz spectral index map. The Hard X-rays are little affected by absorption and indicate the full extent of the SNR. Soft X-ray contours integrated from 0.5-2.6 keV from ASCA (Chen & Slane 2001) superposed on the 74/330 MHz spectral index map are presented in Figure 3b. In contrast to the hard X-rays, the soft X-rays are dramatically absorbed toward the western side of the SNR. This is indicative of an enhanced column density of hydrogen gas (both molecular and neutral) toward the NW and western sides of the SNR compared to the SE as discussed in §1.1. The region of higher column density (indicated by regions with hard X-rays but no soft X-rays) is well correlated with that of the deepest 74 MHz absorption.

### 4.2. Comparison to molecular and atomic line emission

Figure 3c shows CO (2–1) integrated emission contours from 91 to 110 km/s tracing the molecular cloud that is interacting with 3C 391 (Reach & Rho 1999) superposed on the 74/330 MHz spectral index map. The OH (1720 MHz) masers discovered by Frail *et al.* (1996) are also indicated for reference. Much of the CO (2 – 1) emission shown in Figure 3c has narrow line widths, indicating that it has not yet been affected by the shock. Only toward the CO emission peak (near the southern OH maser source) is there obvious evidence for shocked CO gas (Reach & Rho 1999). Figure 3d shows mid infrared emission contours from ISOCAM at 12-18  $\mu\text{m}$  from Reach *et al.* (2002) superposed on the 74/330 MHz spectral index map.

There is impressive agreement between the regions of strongest 74 MHz absorption and the 12-18  $\mu\text{m}$  IR emission shown in Fig. 3d. Such a correlation may seem somewhat unexpected since dust cannot be responsible for the free-free absorption. Indeed, Reach *et*

*al.* (2002) found that the bulk of the infrared emission in the 12-18  $\mu\text{m}$  range toward 3C 391 arises from fine structure atomic [NeII] and [NeIII] infrared lines. These authors also found that the only regions that do have significant dust emission in the 12-18  $\mu\text{m}$  range lie outside of the radio shell (i.e. to the SW and NE; Fig. 3d). In addition to the [NeII] and [NeIII] lines in the 12-18  $\mu\text{m}$  range, Reach *et al.* (2002) also find a similar distribution for [FeII] at 1.64  $\mu\text{m}$  (albeit over a smaller field of view encompassing only the south and western parts of the remnant). Ionized infrared fine structure lines have also been shown to account for much of the 12-25  $\mu\text{m}$  emission observed toward the northeast rim of IC 443; another SNR known to be interacting with a molecular cloud (Oliva *et al.* 1999).

Infrared fine structure lines can be easily formed in the cooling post-shock gas after the passage of a dissociating J-type shock with a speed  $\sim 100 \text{ km s}^{-1}$  (see for example Hollenbach & McKee 1989). Indeed, Reach *et al.* (2002) suggest that since shocked molecular gas as traced by wide CO line widths and excited  $\text{H}_2$  emission is concentrated near the CO peak (Fig. 3c), while the IR line emission is much more widespread (the morphology agrees well with the radio continuum), that much of the shock interaction between the SNR and molecular must be a dissociative J-type shock. This interpretation is supported by the lack of mid-IR continuum or hydrocarbon line emission interior to the remnant, since much of the dust would be destroyed in such a shock (the high abundance of gas phase [Fe] also implies that most of the dust has been destroyed). Thus, the 12-18  $\mu\text{m}$  emission predominately traces the SNR/molecular cloud shock boundaries.

### 4.3. Properties of Free-Free Absorbing Gas

Using Equation 1, and the integrated spectral index found in §3.1 of  $-0.49$ , we derive the following equation for the 74 MHz optical depth as a function of position

$$\tau_{74}(\alpha, \delta) = -\ln \left[ 0.481 \left( \frac{S_{74}(\alpha, \delta)}{S_{330}(\alpha, \delta)} \right) \right], \quad (2)$$

where  $S_{74}(\alpha, \delta)$  and  $S_{330}(\alpha, \delta)$  are the images shown in Figures 1a and 1c. The resulting 74 MHz optical depth map is shown in Figure 4. The morphology of the  $\tau_{74}$  map mimics that of the 74/330 MHz spectral index maps shown in Figures 1 and 3. If the electron temperature is known, the  $\tau_{74}$  map shown in Figure 4 can be converted a map of emission measure ( $EM$ ) using

$$EM = 6.086 \times 10^{-6} a(T_e, \nu)^{-1} \nu^{2.1} \tau(\nu) T_e^{1.35} \text{ cm}^{-6} pc, \quad (3)$$

where  $EM$  is the emission measure,  $T_e$  is the electron temperature (K),  $\nu$  is the frequency in MHz, and  $a(T_e, \nu)$  is the Gaunt factor and is  $\sim 1$  at the temperatures and densities discussed here (Dulk & Snee 1975).



In the remainder of this section we use previous observational data toward 3C 391 (see §4.1 and 4.2) to constrain the properties of the free-free absorbing gas. However, it is important to note that the electron temperature and density (both electron  $n_e$  and total  $n$ ) will change significantly as a function of distance behind the shock front (see for example Hollenbach & McKee 1989). Moreover, since we are observing at least some of the shock front “face-on” (see Fig 3) we are sampling all of these regions along the line of sight simultaneously in a way that cannot be disentangled. Thus, it is impossible to uniquely assign any one value to either  $T_e$  or  $n_e$ . For the remainder of this section we deal only with average or typical values, in order to give a sense of the likely parameter space.

In order to account for the wide range of near infrared, mid-infrared, and molecular lines observed toward 3C 391, Reach & Rho (2000) propose a three component model for the pre-shock gas: atomic (A;  $n_o \sim 1 \text{ cm}^{-3}$ ), molecular (M;  $n_o \sim 100 \text{ cm}^{-3}$ ), and dense clump (C;  $n_o \sim 10^4 \text{ cm}^{-3}$ ). *After passage of the dissociating J-shock*, the primary tracers of each of these components are A: NeIII and OIII ( $n \sim 10 \text{ cm}^{-3}$ ), M: OI, FeII, SiII ( $n \sim 10^3 \text{ cm}^{-3}$ ), and C: H<sub>2</sub>, CS(7-6), and OH (1720 MHz) masers ( $n \sim 10^5 \text{ cm}^{-3}$ ; Reach & Rho 2000; Reach *et al.* 2002). Based on the observed properties of the un-shocked molecular cloud outside of the boundaries of the SNR (Reach & Rho 1999), it seems likely that the majority of the pre-shock gas was composed of component “M” gas. As noted by Reach & Rho (2000), the gas will not of course be segregated into these distinct categories – instead there will be a continuum of these conditions. However, using a number of diagnostics, these authors find that this simple three component model does a good job of reproducing the majority of the observed spectral lines.

Given the excellent morphological agreement between the fine structure ionized atomic line emission and the 74 MHz free-free absorption described in §4.2 (Figure 3d), it seems reasonable to assume that the two tracers coexist. That is that the electrons responsible for the free-free absorption are those created from the ionization of the fine structure line emitting atoms like FeII. By comparing a number of different near and mid-infrared [FeII] lines, Reach *et al.* (2002) find that the line intensities of the iron lines are best fit by a temperature  $\lesssim 3,000 \text{ K}$ . Using this temperature and Equation 3, the average 74 MHz optical depth of 1.1, and  $T_e = 1,000 - 3,000 \text{ K}$  we find that the average  $EM = (0.6 - 2.5) \times 10^3 \text{ cm}^{-6} \text{ pc}$ . However, it is not clear that the ions and electrons would be thermalized as suggested here, especially since the ionization fraction is unknown. In lieu of a better estimate we will assume that  $T_e = 1,000 - 3,000 \text{ K}$ , but the uncertainty of this assumption is inherent in the remaining calculations that use the average  $EM$ .

Likewise, it seems reasonable to assign the post-shock density that is appropriate for the FeII lines of  $n \sim 10^3 \text{ cm}^{-3}$  to the free-free absorption region (i.e. according to the three

component model described above). However, the post-shock electron density ( $n_e$ ) is the key parameter for the free-free absorption and is unknown. In the Reach *et al.* (2002) study, little evidence was found for *shocked* molecular gas (component D, due to dense clumps) with the exception of the region near the southern OH maser (see Fig. 3c). Additionally, little mid-infrared continuum emission was observed in the ISO data, implying wide scale destruction of the dust by the passage of the shock. This conclusion is also supported by the presence of strong gas-phase Fe and Si lines since these species are normally depleted onto grains. From these clues, these authors suggest that much of molecular gas must also have been destroyed by the shock, although there may still be a significant amount of neutral atomic gas present. Indeed, the presence of widespread OI suggests that not everything has been even singly ionized, thus we view  $n \sim 10^3 \text{ cm}^{-3}$  as a strict upper limit to the electron density (also see Oliva *et al.* 1999). It is also possible that some of the free-free absorption arises from the “A” zone (traced by OIII and NeIII), but since we expect  $n_e \sim n \sim 10 \text{ cm}^{-3}$  in this region (see above and Reach & Rho 2000), our  $n_e \lesssim n \sim 10^3 \text{ cm}^{-3}$  upper limit is not violated.

Using  $EM = \int n_e^2 dl$ ,  $n_e \lesssim n \sim 10^3 \text{ cm}^{-3}$  as an upper limit for the electron density, and the emission measure derived above, we find that the thickness of the ionized gas layer responsible for the free-free absorption is  $\gtrsim 0.0006 - 0.0025 \text{ pc}$ . It is notable that some of the free-free absorption could also arise from the “A” zone (traced by OIII and NeIII), but since we expect  $n_e \sim n \sim 10 \text{ cm}^{-3}$  in this region (see above and Reach & Rho 2000), our  $n_e \lesssim n \sim 10^3 \text{ cm}^{-3}$  upper limit is not violated. Unfortunately, previous attempts to model the line emission from J-type shocks either do not include the infrared fine structure lines (Dopita & Sutherland 1996), use pre-shock densities too high for this case ( $n_o > 10^3$ , Hollenbach & McKee 1989), or assume that the pre-shock material is atomic (Hartigan, Raymond, Hartmann 1987) so that these studies cannot be used to predict the parameters of the 3C 391 in detail (see Reach & Rho 2000, for further discussion of these models with regard to 3C 391).

If an independent estimate for the path length for the ionized gas responsible for the free-free absorption can be made, we can estimate the electron density in another way. Chen *et al.* (2004) found that the column density associated with the X-ray absorbing molecular cloud (i.e. the difference in column between the SE and NW parts of the SNR) is  $6 \times 10^{21} \text{ cm}^{-2}$  (see §1.1). Combining this information with the infrared line post-shock density estimate of  $n \sim 10^3 \text{ cm}^{-3}$ , we find that the path length through the X-ray absorbing gas is  $\sim 2 \text{ pc}$ . If we assume that this path length is also appropriate for the ionized gas, and use the average  $EM$  derived above of  $(0.6 - 2.5) \times 10^3 \text{ cm}^{-6} \text{ pc}$ , we find that  $n_{e,avg} \sim 20 - 40 \text{ cm}^{-3}$ . However, there could be a significant contribution to the molecular cloud column density (determined from the differential x-ray absorption) by un-shocked gas of lower density than

assumed here. Since it is not possible to quantify this effect (high resolution HI absorption measurements would be useful but do not exist), it is not clear how significant this estimate is. Another independent assessment of the thickness of the ionized gas layer can be made from the transverse size scale over which there are significant changes in the 74 MHz free-free absorption. From Figures 3 and 4, this sizescale is  $1' - 2'$  which corresponds to 2.2 to 4.4 pc at a distance of 7.5 kpc. If we make the usual assumption that the depth is approximately equal to the transverse sizescale, the electron density is  $n_{e,avg} \sim 10 - 35 \text{ cm}^{-3}$  in good agreement with that determined from the X-ray column density path length.

Electron densities of  $10 - 40 \text{ cm}^{-3}$  are consistent with the suggestion of Reach & Rho (2000) that  $n_e \sim n/100 \text{ cm}^{-3}$ , if the post-shock density is  $\sim 10^{3-3.5} \text{ cm}^{-3}$ . This range of electron densities is somewhat higher than typically assumed in other studies of free-free absorption derived from integrated flux measurements (e.g.  $1 - 10 \text{ cm}^{-3}$  Kassim 1989b; Dulk & Slee 1975). However, we also assume an electron temperature that is somewhat lower:  $1,000 - 3,000 \text{ K}$  compared to the  $3,000 - 8000 \text{ K}$  typically assumed, so that the implied pressure is similar. The lower temperature estimated here also seems reasonable in light of the fact that the  $3,000 - 8000 \text{ K}$  estimate from Kassim (1989b) is appropriate for the extended envelopes of H II regions, i.e. photoionization, compared to the predominately collisional ionization suggested here for 3C 391.

#### 4.4. Nature of the 3C 391 74 MHz Absorption

The nature of the medium that causes free-free thermal absorption toward the large number of SNRs observed to have low frequency spectral turnovers remains uncertain (c.f. Kassim 1989b). For example, two obvious sources of Galactic ionized gas: the warm ionized medium (WIM) and H II regions do not provide the appropriate physical conditions to account for most of the SNRs with thermal absorption. The WIM has electron densities that are too low by a factor of  $\sim 10$  to  $100$  and its filling factor is too high ( $\sim 20\%$ ; Kulkarni & Heiles 1987; Reynolds 1991). This last is important because Kassim (1989b) showed that SNR free-free absorption is not correlated with distance, as would be necessary for a ubiquitous distributed component like the WIM. Normal H II regions have electron densities and temperatures that are too high to account for the moderate low frequency optical depths that are observed ( $\tau_{74} \sim 1$ ) toward most SNRs with thermal absorption, although there are a few cases with very high optical depths where this is a likely scenario (W30 for example).

Two viable alternatives for intermediate temperature and density ionized thermal gas have been suggested. Anantharamaiah (1985, 1986) has suggested that the extended envelopes of normal H II regions (EHEs) might well provide the requisite temperatures and

densities. This suggestion was prompted by the statistical correlation of high and low frequency RRL velocities, indicating that they may arise from the same kinematic regions. However, it is unclear whether such envelopes extend far enough into the ISM to account for a large fraction of the SNRs showing low frequency absorption. Alternatively, Heiles, Reach, & Koo (1996) suggest that Galactic “worms” may cause absorption toward some sources. Ionized “worms” occur when a later generation of massive OB stars ionizes a preexisting superbubble. Indeed, the absorption observed toward the SNR W49B by Lacey *et al.* (2001) may be due to such a “worm” (Brogan *et al.* 2004). However, the physical properties of “worms” are not currently well determined so it is not clear whether they can account for a large number of SNR thermal absorption cases.

*The free-free absorption observed toward 3C 391 provides the first evidence for another origin: ionized gas produced when a SNR blast wave encounters a nearby molecular cloud with sufficient speed to dissociate and ionize the gas.* This is an exciting prospect since it implies that the large fields of view afforded by low radio frequency observations may be used to efficiently search for cases of SNR/molecular cloud interactions. Thus far only a handful of such cases are known from traditional blind HI and CO surveys (for example W44, IC443, W28, and HB21, Reach *et al.* 2002, and references therein), despite the fact that it seems plausible that many SNRs should still be located in or near their nascent molecular clouds. OH (1720 MHz) masers, found toward  $\sim 10\%$  of SNRs, have proven to be powerful signposts of SNR/molecular cloud interactions (Green *et al.* 1997). A number of new interaction cases have been confirmed by follow-up infrared and mm-wavelength observations of SNRs with OH (1720 MHz) masers, including 3C 391 (also see for example Lazendic *et al.* 2004; Reynoso & Mangum 2000). However, these masers require a very limited set of physical conditions to be pumped (i.e. slow C-type shocks with  $T \sim 100$  K and  $n \sim 10^4$  cm $^{-3}$  Wardle 1999), so that while molecular gas must be present where they are found, non-detection is inconclusive. Thus, low frequency free-free thermal absorption may provide an important complementary tracer of fast ionizing SNR/molecular cloud shocks. Unfortunately, since typical HI clouds in the cold neutral medium (CNM) only have densities of  $\sim 0.5$  cm $^{-3}$  (see for example Heiles & Troland 2003), it is unlikely that SNR/CNM HI clouds interactions would produce observable free-free absorption.

One obvious benefit to be gained by finding more SNR/molecular cloud interactions, is that the velocity of the cloud can then be used to derive a kinematic distance for the remnant. In this regard, radio recombination line detections of the free-free ionized gas would also yield velocity information. SNRs distances are notoriously difficult to obtain although it is a key parameter in most SNR diagnostics like physical size, age, and energetics. Given the low number of SNRs for which accurate distance estimates exist, even a few new free-free absorption driven SNR/molecular cloud discoveries would represent a significant gain.

For currently known examples of SNR/molecular cloud interaction, free-free absorption also represents an important means of studying the properties of the shock, since only J-type shocks can create the requisite ionized gas. However, it is also notable that if the free-free absorption observed toward 3C 391, is common toward SNRs with associated molecular clouds, the observation of intrinsic spectral index variation due to shock acceleration will be very difficult to detect at low radio frequencies.

## 5. CONCLUSIONS

For the first time we have been able to spatially resolve (at  $70''$  resolution) the morphology of the low frequency free-free absorption toward 3C 391, previously inferred from integrated flux measurements. We find that the average 74 MHz optical depth is 1.1 and the spectral index of the SNR is  $-0.49$ . There is impressive agreement between the regions of strongest 74 MHz free-free absorption and ionized fine structure atomic lines between 12-18  $\mu\text{m}$ . This coincidence suggests that the source of ionized thermal gas responsible for the low frequency absorption arises from the SNR/molecular cloud shock boundary. The appropriate range of temperatures and densities to excite the fine structure lines can be easily achieved in the post-shock gas of a J-type shock with a speed of  $\sim 100 \text{ km s}^{-1}$  (Reach *et al.* 2002). Using the range of temperatures appropriate for the infrared ionized fine structure lines of 1,000 – 3,000 K (Reach *et al.* 2002) we find that the average emission measure of the free-free absorbing gas is  $EM = (0.6 - 2.5) \times 10^3 \text{ cm}^{-6} \text{ pc}$ . From a number of different lines of evidence including the infrared fine structure emission and the observed differential X-ray absorption across 3C 391, we find that the electron density likely lies between  $10 - 10^3 \text{ cm}^{-3}$ , with a lower range between  $10 - 40 \text{ cm}^{-3}$  favored.

A study by Kassim (1989b) suggested that  $\sim 2/3$  of all SNRs in the Galaxy suffer from some degree of low frequency free-free absorption. It has been proposed that such absorption is due to a *diffuse* ( $n_e \sim 1 - 10 \text{ cm}^{-3}$ ) ionized component of the ISM - possibly the extended envelopes of H II regions. This new work shows for the first time that such absorption can arise from ionized gas in the post-shock region behind a SNR/molecular cloud shock interface. This result is in direct contrast to the result of Lacey *et al.* (2001) for the SNR W49B where the low frequency absorption was shown to be linked to an unrelated kinematic component along the line of sight. Additionally, the electron temperatures ( $\sim 1,000 - 3,000 \text{ K}$ ) associated with the thermal ionized gas surrounding 3C391 is lower than the canonical values (3,000 – 8,000 K) assumed by previous interpretations of thermal ISM absorption (see for example Kassim 1989b).

Our result implies that thermal absorption effects towards SNR/molecular cloud com-

plexes may be significantly stronger than previously suspected, if J-type shocks are common. This is only the second case after W49B for which *extrinsic* free-free thermal absorption toward an SNR has been spatially resolved (free-free absorption from thermal gas interior to a remnant has also been observed toward CasA and the Crab). Future spatially resolved VLA 74 MHz studies toward a larger sample of Galactic SNRs from our ongoing VLA 74 MHz inner Galactic plane survey ( $l = -10^\circ$  to  $50^\circ$ ; Brogan et al. 2004, in prep.) will be a powerful tool in the search for elusive SNR/molecular cloud interactions. They will also allow us to study the prevalence of the other possible sources of free-free absorption described in §4.4. The next generation of low frequency instruments like the Long Wavelength Array (LWA) and the Low Frequency Array LOFAR, with their superior resolution and sensitivity will likely shed even greater light on this phenomenon.

We would like to thank S. P. Reynolds for giving us permission to utilize his archival VLA 330 and 1465 MHz data. We would also like to thank W. Reach for supplying us with his CO and IR data in electronic form. Likewise for P. Slane for supplying us with the X-ray data. We would also like to thank the anonymous referee for helping us to improve the clarity of the text. Basic research in radio astronomy at the NRL is supported by the Office of Naval Research. KKD acknowledges support during this research as an NSF Astronomy and Astrophysics Postdoctoral Fellow under award AST-0103879 and currently as a National Research Council Postdoctoral Fellow.

## REFERENCES

- Anantharamaiah, K. R. 1985, *Journal of Astrophysics and Astronomy*, 6, 203
- Anantharamaiah, K. R. 1986, *Journal of Astrophysics and Astronomy*, 7, 131
- Brogan, C. L., Devine, K. E., Lazio, T. J., Kassim, N. E., Tam, C. R., Briske, W. F., Dyer, K. K., & Roberts, M. S. E. 2004, *AJ*, 127, 355
- Cesarsky, D. A. & Cesarsky, C. J. 1973, *ApJ*, 184, 83
- Chen, Y. & Slane, P. O. 2001, *ApJ*, 563, 202
- Chen, Y., Su, Y. Slane, P. O., & Wang, Q. D. 2004, *ApJ*, in press, Astro-ph/0408355
- Dopita, M. A. & Sutherland, R. S. 1996, *ApJS*, 102, 161
- Dulk, G. A. & Slee, O. B. 1975, *ApJ*, 199, 61

- Frail, D. A., Goss, W. M., Reynoso, E. M., Giacani, E. B., Green, A. J., & Otrupcek, R. 1996, *AJ*, 111, 1651
- Green, A. J., Frail, D. A., Goss, W. M. , & Otrupcek, R. 1997, *AJ*, 114, 2058
- Hartigan, P., Raymond, J., & Hartmann, L. 1987, *ApJ*, 316, 323
- Heiles, C., Reach, W. T., & Koo, B. 1996, *ApJ*, 466, 191
- Heiles, C., & Troland, T. H. 2003, *ApJ*, 586, 1067
- Hollenbach, D. & McKee, C. F. 1989, *ApJ*, 342, 306
- Jones, T. W. *et al.* 1998, *PASP*, 110, 125
- Kassim, N. E. 1989, *ApJ*, 347, 915
- Kassim, N. E. 1989, *ApJS*, 71, 799
- Kassim, N. E. 1992, *ApJ*, 103, 943
- Kulkarni, S. R. & Heiles, C. 1987, *ASSL Vol. 134: Interstellar Processes*, 87
- Lacey, C. K., Lazio, T. J. W., Kassim, N. E., Duric, N., Briggs, D. S., & Dyer, K. K. 2001, *ApJ*, 559, 954
- Lazendic, J. S., Wardle, M., Burton, M. G., Yusef-Zadeh, F., Green, A. J., & Whiteoak, J. B. 2004, *MNRAS*, 354, 393
- Moffett, D. A. & Reynolds, S. P. 1994, *ApJ*, 425, 668
- Oliva, E., Moorwood, A. F. M., Drapatz, S., Lutz, D., & Sturm, E. 1999, *A&A*, 343, 943
- Oliva, E., Lutz, D., Drapatz, S., & Moorwood, A. F. M. 1999, *A&A*, 341, L75
- Pankonin, V. & Downes, D. 1976, *A&A*, 47, 303
- Radhakrishnan, V., Goss, W. M., Murray, J. D., & Brooks, J. W. 1972, *ApJS*, 24, 49
- Reach, W. T. & Rho, J. 1999, *ApJ*, 511, 836
- Reach, W. T. & Rho, J. 2000, *ApJ*, 544, 843
- Reach, W. T., Rho, J., Jarrett, T. H., & Lagage, P. 2002, *ApJ*, 564, 302

- Reich, W., Furst, E., Steffen, P., Reif, K., & Haslam, C. G. T. 2001, *VizieR Online Data Catalog*, 405, 80197
- Reich, W., Reich, P., & Furst, E. 1997, *VizieR Online Data Catalog*, 408, 30539
- Reynolds, R. J. 1991, *ApJ*, 372, L17
- Reynolds, S. P. & Ellison, D. C. 1992, *ApJ*, 399, L75
- Reynolds, S. P. & Moffett, D. A. 1993, *AJ*, 105, 2226
- Reynoso, E. M. & Mangum, J. G. 2000, *ApJ*, 545, 874
- Rho, J.-H. & Petre, R. 1996, *ApJ*, 467, 698
- Rho, J. & Petre, R. 1998, *ApJ*, 503, L167
- Roshi, D. A. & Anantharamaiah, K. R. 2001, *ApJ*, 557, 226
- Torres, D. F., Romero, G. E., Dame, T. M., Combi, J. A., & Butt, Y. M. 2003, *Phys. Rep.*, 382, 303
- Wang, Z. R. & Seward, F. D. 1984, *ApJ*, 279, 705
- Wardle, M. 1999, *ApJ*, 505, L101
- Wilner, D. J., Reynolds, S. P., & Moffett, D. A. 1998, *AJ*, 115, 247



Table 1. VLA Observational Parameters

| Date                             | Config. | Bandwidth<br>(MHz) | Time <sup>a</sup><br>(Hours) |
|----------------------------------|---------|--------------------|------------------------------|
| 74 MHz parameters                |         |                    |                              |
| 2000 Dec 31                      | A       | 1.5                | 1.33                         |
| 2001 Jan 13                      | A       | 1.5                | 1.33                         |
| 2001 Mar 01                      | B       | 1.5                | 1.7                          |
| 2001 Aug 28                      | C       | 1.5                | 1.0                          |
| 330 MHz parameters <sup>b</sup>  |         |                    |                              |
| 1994 Oct 23                      | C       | $3.1 \times 2$     | 2.5                          |
| 1465 MHz parameters <sup>c</sup> |         |                    |                              |
| 1991 Apr 12                      | D       | $6.25 \times 2$    | 1.25                         |

<sup>a</sup>Approximate time on source

<sup>b</sup>Archival VLA data from project AR311

<sup>c</sup>Archival VLA data from project AR232

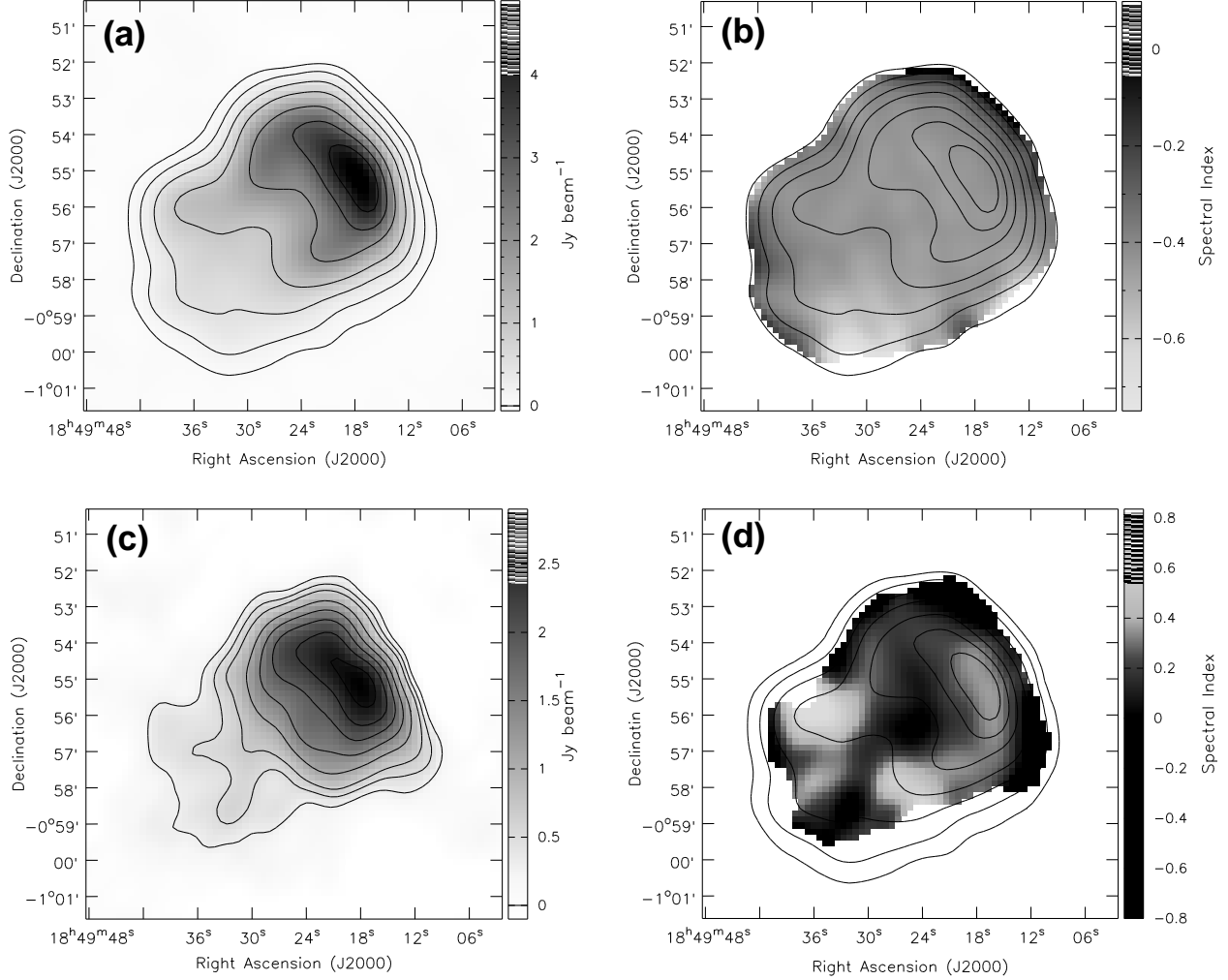


Fig. 1.— (a) VLA 330 MHz continuum image of 3C 391 with 70'' resolution and contours at 0.06, 0.2, 0.5, 1, 2, 3, & 4 Jy beam<sup>-1</sup>. The rms noise of this image is 0.015 Jy beam<sup>-1</sup>. (b) Spectral index map of 3C 391 between 330/1465 MHz. The 330 MHz continuum contours from (a) are superposed. The spectral index is quite uniform with an average value of  $-0.45$ . (c) VLA 74 MHz continuum image of 3C 391 with contours at 0.3, 0.5, 0.7, 1.1, 1.5, 1.9, 2.3, and 2.7 Jy beam<sup>-1</sup> (the rms noise is 0.075 Jy beam<sup>-1</sup>). (d) Spectral index map of 3C 391 between 74/330 MHz. The 330 MHz continuum contours from (a) are superposed. Note that the spectral indices are inverted (positive) over much of the map (the grey scale is also inverted compared to (b)).

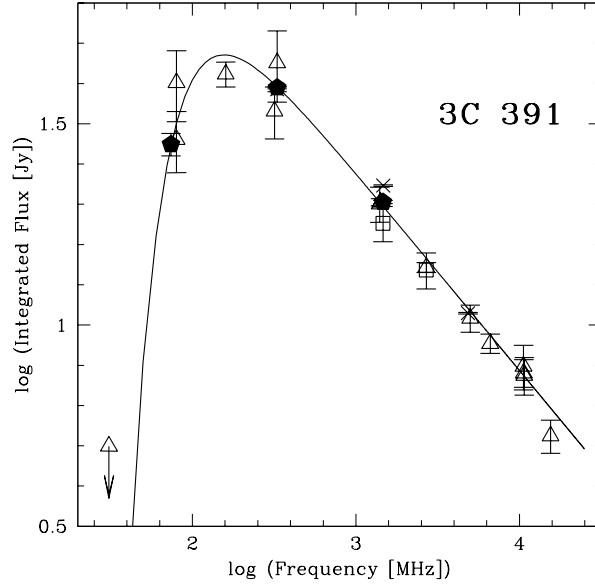


Fig. 2.— Radio continuum spectrum for SNR 3C 391. The solid line is the fit to the data using Equation 1 excluding the 30.9 MHz upper limit. The fitted spectral index is  $-0.49 \pm 0.01$ . The filled hexagon symbols are from the current work, the  $\triangle$  symbols are from Kassim (1989a, 1992), the  $\square$  symbols are from Reich et al. (2001) and Reich, Reich, & Furst (1997), while the  $\times$  symbols are from Moffett & Reynolds (1994).

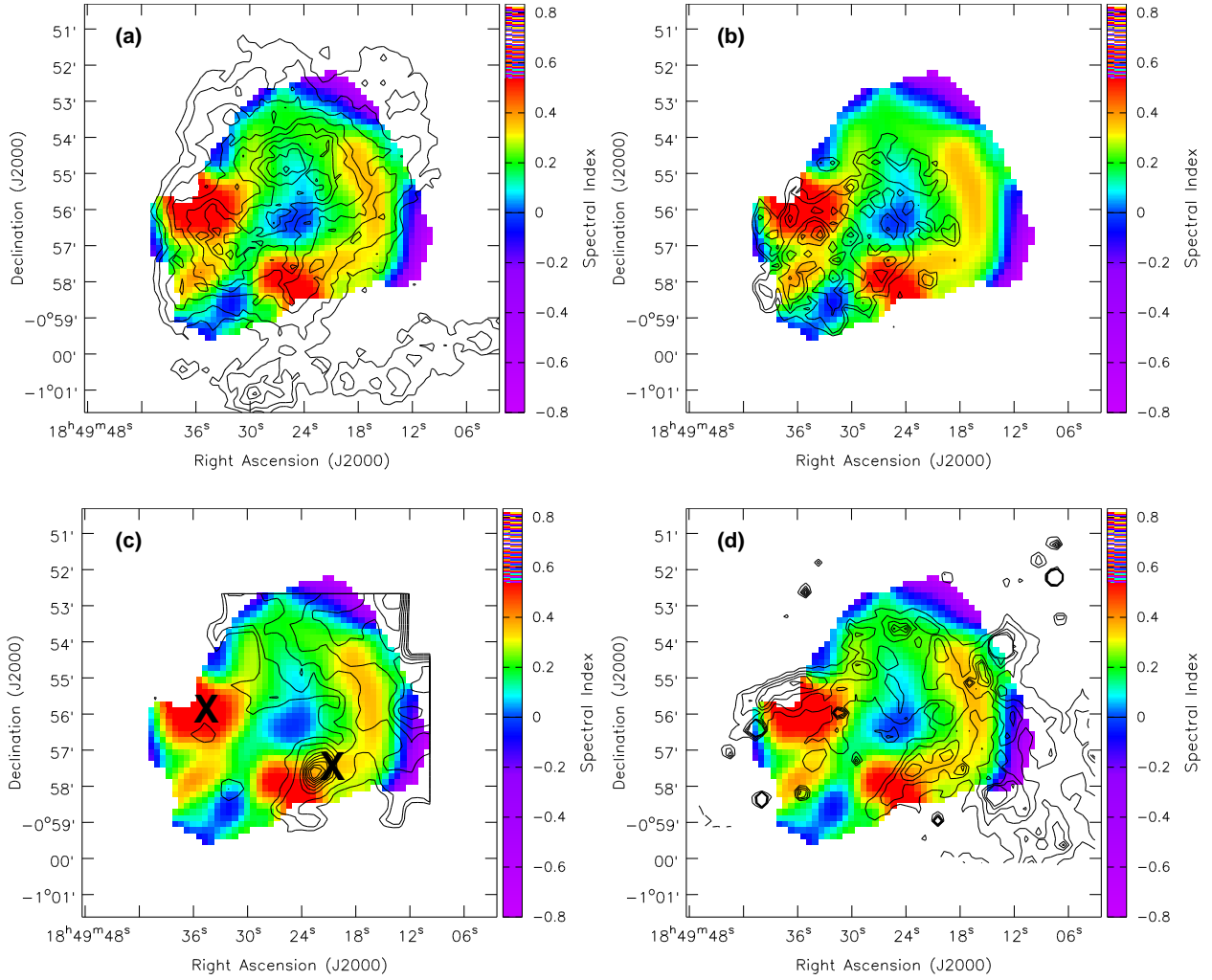


Fig. 3.— Color version of the 74/330 MHz spectral index map presented in Figure 1d superposed with (a) Hard X-ray contours from ASCA in the 2.6-10 keV range Chen & Slane (2001); (b) Soft X-ray contours from ASCA in the 0.5-2.6 keV range (Chen & Slane 2001); (c) CO (2-1) integrated emission contours from 91 to 110 km s<sup>-1</sup> tracing the molecular cloud interacting with 3C 391 (Reach & Rho 1999); and (d) IR emission contours from ISOCAM at 12-18 μm (Reach *et al.* 2002). The × symbols on (c) indicate the positions of OH (1720 MHz) masers (Frail *et al.* 1996). There is impressive agreement between the regions of strongest 74 MHz absorption and the IR emission.

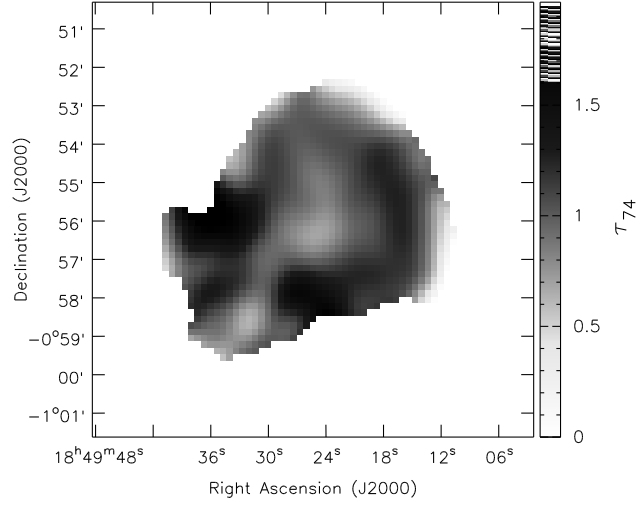


Fig. 4.— Optical depth toward 3C 391 at 74 MHz as a function of position. The  $\tau_{74}$  optical depth was calculated using Equation 2, assuming a constant spectral index of  $-0.49$ . Using this map along with an estimate of the electron temperature, the 74 MHz emission measure ( $EM$ ) can be calculated from Equation 3 ( $EM = 0.051 \tau_{74} T_e^{1.35} \text{ cm}^{-6} \text{ pc}$ ).